Pol. J. Environ. Stud. Vol. XX, No. X (XXXX), 1-13
DOI: 10.15244/pjoes/225300 ONLINE PUBLICATION DATE: 2026-09-02

Original Research

Mechanisms of Environmental Factors Influencing CO_2, CH_4, and N_2O Emissions under Intermittent Irrigation in Coastal Rice Fields of Northern Zhejiang, China

Cheng Lu[1, 2], Menghua Xiao[2], Shizong Zheng[2], Lei Wang[2], Yuanyuan Li[3]*, Yu Jin[2], Mingjie Hu[1, 2], Wanyong Huang[2], Hongwei Jia[2]

[1]College of Agricultural Science and Engineering, Hohai University, Nanjing 211100, China
[2]Zhejiang Institute of Hydraulics and Estuary (Zhejiang Institute of Marine Planning and Design), Hangzhou 310020, China
[3]School of Water Conservancy, North China University of Water Resources and Electric Power, Zhengzhou 450045, China

Received: 12 February 2026
Accepted: 30 June 2026

Abstract

Environmental conditions significantly affect greenhouse gas (GHG) emissions from rice paddies. Using an open-path monitoring system, this study investigated methane (CH_4), carbon dioxide (CO_2), and nitrous oxide (N_2O) emissions from intermittently irrigated coastal rice fields in northern Zhejiang, China. The results revealed synchronized trends in air, soil, and rice canopy temperatures, all peaking at the late tillering stage. Gross primary production (GPP) and net ecosystem production (NEP) showed similar dynamics, with cumulative values of 850.51 and 294.36 g C/m^2, respectively. Both GPP and NEP showed linear positive correlations with photosynthetically active radiation (PAR) and a quadratic relationship with vapor pressure deficit (VPD). CH_4 emissions peaked at tillering, with daily fluxes of 0.02-1.19 g/m^2/d and a total of 27.05 g/m^2. Positive linear correlations were observed between CH_4 emissions and temperature as well as VPD, explaining 15.12-17.37% and 10.14% of CH_4 variation, respectively. The average N_2O flux was 2.5281 μg·m^{-2}·h^{-1}, with higher cumulative fluxes during the jointing and booting stages. These results clarify GHG emission characteristics in northern Zhejiang's rice fields and support the development of mitigation strategies.

Keywords: rice fields, environmental factors, GPP and NEP, CH_4 and N_2O, structural equation model

*e-mail: liya66720@126.com
0000-0001-9061-6885

Introduction

Rice is a staple grain crop in China, where it occupies approximately 20% of the global rice cultivation area. Rice production is a major consumer of water and fertilizers and a significant source of carbon emissions [1]. Direct carbon emissions during rice cultivation, primarily in the form of CO_2, CH_4, and N_2O, account for about 70% of the total emissions from rice production. Among these gases, CO_2 and CH_4 account for 86% and 16% of the total greenhouse effect, respectively [2-4]. With increasing rice demand driven by population growth and economic development, CH_4 emissions from rice fields are expected to rise continuously. Alternate wetting and drying (AWD), a water-saving irrigation method, modifies soil moisture through periodic wetting and drying cycles, significantly altering the redox environment, microbial activity, and carbon-nitrogen cycling processes, thereby regulating greenhouse gas (GHG) emissions [5, 6]. Thus, understanding the coupling relationship between dynamic environmental factors and GHG emissions under AWD is crucial for reducing emissions from rice fields.

The CO_2 flux in paddy fields is closely linked to gross primary production (GPP) and net ecosystem production (NEP) [7]. Previous studies have reported that carbon fluxes in agroecosystems are primarily regulated by environmental factors such as radiation, temperature, and precipitation, as well as crop varieties, leaf area index, and nutrient availability [8, 9]. However, the dominant environmental factors influencing daily NEP variations may differ among years with different climatic conditions. For instance, some studies suggest that air temperature and vapor pressure deficit (VPD) have a greater impact on daily NEP than photosynthetically active radiation (PAR) [10]. Environmental factors also affect CH_4 emission dynamics in rice fields. Previous research indicates that air temperature is the primary factor controlling seasonal CH_4 emission variations, with VPD as a secondary factor [11]. Another study demonstrated that daily CH_4 emissions could be significantly influenced by air temperature, soil moisture content, net radiation, and VPD, while hourly CH_4 emissions showed highly significant relationships with air temperature, radiation, and VPD [12]. Studies have also found that air temperature, water temperature, and atmospheric pressure are the primary influencing factors for greenhouse gas emissions. Temperature significantly affects the emissions of CO_2, CH_4, and N_2O. Solar radiation accelerates organic matter decomposition by increasing soil temperature, creating a synergistic effect that enhances GHG emissions. CH_4 emissions are influenced by wind speed, showing a positive correlation [13, 14]. Soil temperature regulates N_2O emissions and significantly affects carbon-nitrogen transformation rates [15]. Changes in soil temperature and moisture explained 52.0-58.2% and 60.7-71.4% of N_2O emissions, respectively. N_2O emissions showed significant positive correlations with soil organic carbon, microbial biomass carbon, total nitrogen, and pH, while exhibiting a significant negative correlation with soil bulk density [16]. Based on the above findings, environmental factors play a crucial regulatory role in carbon and nitrogen fluxes in agricultural systems. However, existing research has largely focused on individual greenhouse gases or specific environmental factors, leaving a significant gap in the systematic identification of key environmental drivers and the synergistic response mechanisms that govern multiple greenhouse gas emissions. In particular, the differential regulatory patterns of environmental factors on multi-gas emissions across different temporal scales (e.g., diurnal and seasonal variations) remain unclear.

The coastal rice fields in northern Zhejiang face challenges of increasing irrigation water consumption and negative environmental impacts from excessive fertilization. Rice production in this region accounts for about 40% of provincial water use and 70% of chemical fertilizer use, primarily nitrogen fertilizers, and contributes to approximately 20% of the provincial agricultural GHG emissions [17, 18]. The average temperature, wind speed, and sunshine duration in this region differ significantly from those in inland areas, leading to patterns of GHG emissions and carbon sequestration mechanisms that differ from those in traditional inland rice fields [19]. Furthermore, extreme weather events such as typhoons and heavy rainfall, combined with hydrological fluctuations caused by tidal effects, lead to greater complexity in the dynamics of water and carbon pools (e.g., straw decomposition, soil organic carbon transformation) and nitrogen cycling (e.g., fertilizer uptake, nitrification-denitrification) [20]. As a result, the patterns of greenhouse gas emissions and carbon sequestration mechanisms in these coastal rice fields differ significantly from those in traditional inland rice fields.

To investigate GHG emission patterns and explore the impacts of environmental factors under AWD irrigation in coastal rice-growing areas of northern Zhejiang, field-based experiments were conducted to monitor water and carbon fluxes, CH_4 and N_2O emissions, and environmental factors in rice fields. The objectives were to (i) assess the current state of GHG emissions from rice fields, (ii) identify key environmental factors regulating GHG production, emission, and absorption under water-saving irrigation, and (iii) explore the influencing mechanisms of these factors. These findings enhance understanding of the roles of environmental factors in GHG emissions during rice production and contribute to optimizing water-carbon-nitrogen management in rice-producing areas to mitigate the greenhouse effect caused by agricultural practices.

Materials and Methods

Experimental Site

Field experiments were conducted during the rice season (June to October 2024) at the Zhejiang Provincial Irrigation Experiment Center Station (120°39′E, 30°18′N, average elevation 7.0 m). The experimental area has a uniform underlying surface, with a local annual average precipitation of 1320.5 mm, average temperature of 16.1ºC, frost-free period of 224 days, relative humidity of 82%, sunshine duration of 2116.6 hours, and annual radiation of 109.6 kcal/m^2. The soil is sandy loam, with an original soil organic matter content of 1.1%, total nitrogen (TN) of 0.06%, total phosphorus (TP) of 0.06%, pH of 7.5, and salt content of 0.1-0.2%. The experimental site is representative of the Hangjiahu Plain and coastal areas of northern Zhejiang Province (Fig. 1).

Experimental Design

Seedlings of the rice variety Zhenghexiang No. 2 were transplanted at a hill spacing of 25 cm × 15 cm on June 21, and the crop was harvested on October 29, 2024. A randomized block design was used with three replications of equal size. The growth stages were divided as shown in Table 1. The total growth cycle lasted 131 days, with vegetative and reproductive growth periods lasting 41 days and 90 days, respectively. Rice fields were irrigated following an intermittent irrigation practice, maintaining a cycle of shallow flooding, moist conditions, and short drying periods. The upper and lower moisture limits were monitored using a vertical ruler installed in the measuring bucket and a TDR instrument. Detailed water management information is provided in Table 2. Fertilization followed local management practices, as detailed in Table 3.

Greenhouse Gas Measurement and Environmental Factor Monitoring

CH_4, CO_2, and H_2O fluxes were monitored using an open-path eddy covariance system (LI-7500DS, LI-COR, USA) (Fig. 2). The system automatically retrieved raw flux data, along with gas analyzer and ultrasonic anemometer data, to calculate and output CH_4 and CO_2 fluxes. N_2O samples were collected using the static dark box method, with gas samples analyzed by gas chromatography (Fig. 3). Conventional

Fig. 1. Experimental site.

Table 1. The growth stages of rice.

2024	Vegetative stage			Reproductive growth stage			
	Regreening	Early tillering	Late tillering	Jointing–booting	Heading –flowering	Milky stage	Maturity
Date	6.21-7.04	7.05-7.14	7.15-7.31	8.01-9.03	9.04-9.13	9.14-10.09	10.10-10.29
Duration (days)	14	10	17	34	10	26	20

Table 2. Water-layer control standards for paddy fields.

Irrigation water level regulation	Vegetative stage			Reproductive growth stage			
	Regreening	Early tillering	Late tillering	Jointing–booting	Heading–flowering	Milky stage	Maturity
Lower limit of irrigation (mm)	5	$0.8\theta_s$	$0.7\theta_s$	$0.9\theta_s$	0	$0.8\theta_s$	Natural drying
Upper limit of irrigation (mm)	30	20	20	30	30	20	
Upper limit of rainwater storage (mm)	50	70	0	120	100	60	

Table 3. Fertilization regime during growth stages.

Fertilizer type (date)	Basal fertilizer (Jun 19)	Topdressing during the vegetative growth stage				Topdressing during the reproductive growth stage (Aug 6)
		First (Jul 2)	Second (Jul 9)	Third (Jul 16)	Fourth (Jul 23)	
Total (kg/ha)	185	148	165	262	222	222
N (kg/ha)	28	/	/	39	/	
P_2O_5 (kg/ha)	28	/	/	39	/	
K_2O (kg/ha)	28	/	/	39	/	
Urea (kg/ha)	/	148	165	/	222	222

Fig. 2. Open-path greenhouse gas flux monitoring system.

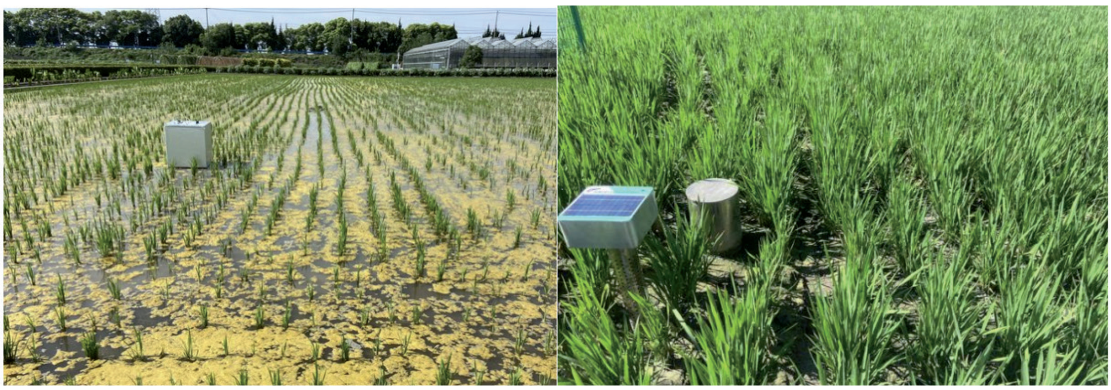

Fig. 3. Static chamber N_2O sampling and rice cultivation experiment.

meteorological indicators, including air temperature (Ta), soil temperature (Ts), canopy temperature (T_leaf), PAR, VPD, and wind speed (v), were monitored using a weather station and the open-path eddy covariance system.

Results

Dynamic Changes in Environmental Factors

The dynamic changes in air temperature (Ta), soil temperature (Ts), canopy temperature (T_leaf), photosynthetically active radiation (PAR), vapor pressure deficit (VPD), and wind speed (v) in the rice fields are shown in Fig. 4. As depicted in Fig. 4a), Ta, Ts, and T_leaf exhibited similar trends. Following rice sowing in June, Ta progressively rose, accompanied by corresponding increases in Ts and T_leaf, peaking in July at the end of the regreening stage, with values reaching 34.65ºC, 33.29ºC, and 31.05ºC, respectively. Throughout the tillering stage, these temperatures displayed significant fluctuations, initially decreasing, then increasing, and finally decreasing again, attaining their maximum values during the growth cycle. Specifically, by the end of the tillering stage (August 3rd), Ta, Ts, and T_leaf peaked at 34.99ºC, 33.42ºC, and 32.71ºC, respectively. During the jointing-booting and flowering stages, a gradual decline was observed, while the grain-filling stage saw a slight uptick followed by a steady decrease until harvest. In the initial phase, from transplanting to the tillering stage, the low leaf area index and low canopy coverage resulted in T_leaf primarily reflecting the water surface temperature, rendering it lower than both Ta and Ts. As the canopy matured, T_leaf aligned with Ta. During the entire growth period, Ta ranged from 15.60 to 34.99ºC, averaging 27.64ºC. Ts spanned 18.03 to 33.42ºC, averaging 27.48ºC. T_leaf varied from 15.00 to 32.71ºC, averaging 25.2ºC.

The spectral composition of the radiation under study fell exclusively within the 0.4-0.7 µm wavelength range of total solar radiation (Fig. 4b)), serving as the primary energy driver for rice photosynthesis and directly influencing its photosynthetic processes, growth, and development. The photosynthetically active radiation (PAR) exhibited a sawtooth fluctuation pattern, peaking at 574.6 mol/m^2/d from rice transplanting to the end of regreening. During the tillering stage, PAR showed large fluctuations, then gradually declined with minor undulations until reaching its minimum at harvest. Across the growth period, PAR ranged from 3.35 to 49.65 mol/m^2/d, averaging 28.6 mol/m^2/d. This variation stemmed from changes in the intensity and direction of solar radiation reaching the rice canopy, which were influenced by shifts in the solar altitude angle, thereby affecting PAR distribution. Moreover, alterations in wind direction and speed modified the airflow within the canopy, impacting leaf temperature and humidity, and consequently, the efficiency of PAR

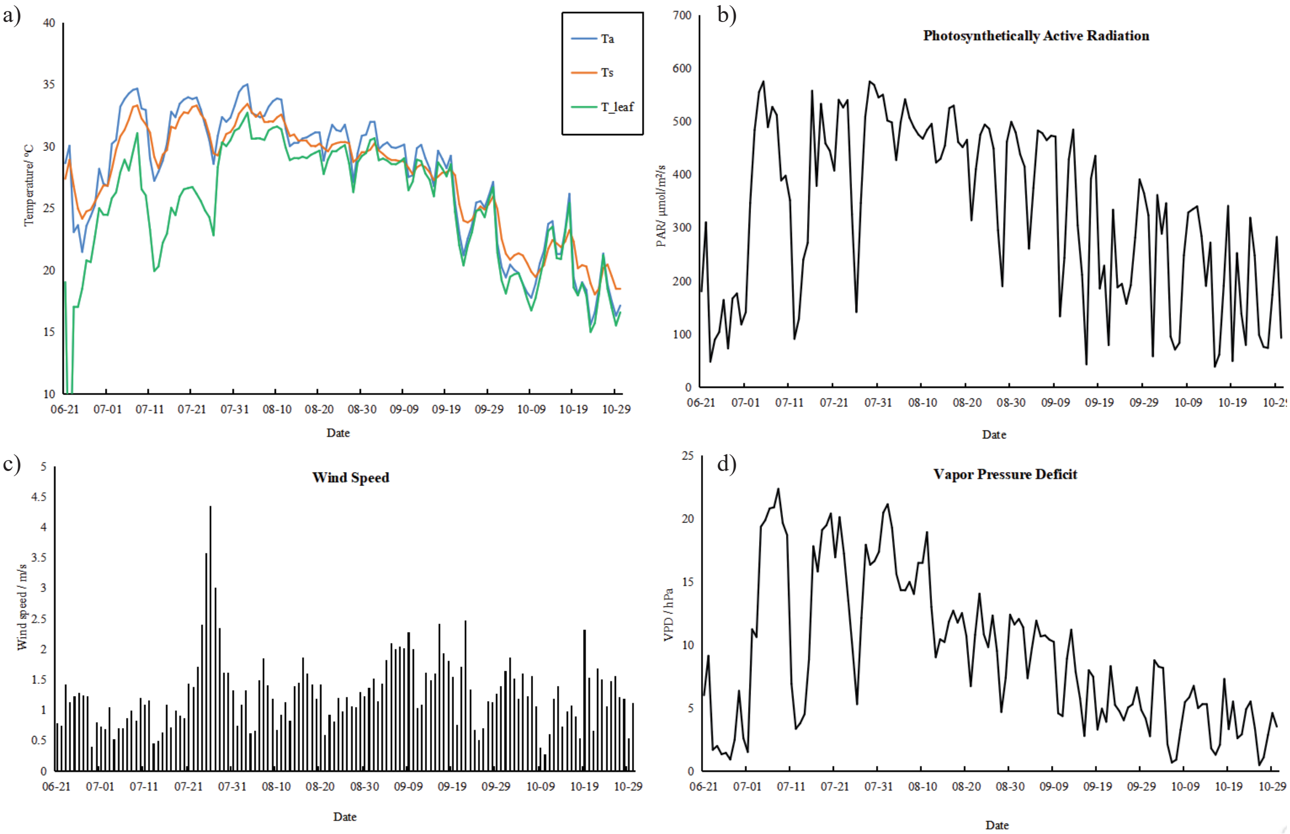

Fig. 4. Dynamic changes in environmental factors.

utilization. Wind speed and direction varied with season and weather conditions. Fig. 4c) reveals that, in summer, high temperatures and low air pressure led to relatively high wind speeds, peaking at 4.36 m/s in late July (late tillering stage). Conversely, winter wind speeds were lower due to cold temperatures and high air pressure, with wind conditions fluctuating in other months. Fig. 4d) illustrates that the vapor pressure deficit (VPD) exhibited significant daily fluctuations, strongly influenced by climatic conditions, particularly when light was abundant during the tillering stage in July. From the jointing–booting stage onwards, VPD fluctuations diminished, showing a gradual decline. VPD levels were higher on sunny days and dropped sharply on cloudy or rainy days. Over the entire growth period, VPD ranged from 0.4 to 22.34 hPa.

GPP and NEP Variation Patterns

Fig. 5 presents the dynamic and cumulative changes in Gross Primary Productivity (GPP) and Net Ecosystem Productivity (NEP) during the rice-growing season. GPP displayed distinct stage-specific variations: Initially, from transplanting to tillering, rice root damage temporarily reduced photosynthetic capacity, leading to a GPP decline. Over time, root recovery prompted a gradual GPP increase. From tillering to jointing, leaf proliferation and expanded photosynthetic area resulted in a significant GPP rise. From jointing to heading, photosynthates primarily supported grain formation, with GPP continuing to climb. From heading to the milky stage, rapid grain development and substantial photosynthate accumulation drove GPP to peak at 14.07 g $C/m^2/d$ on August 22. Subsequently, from the milky stage to maturity, as grains matured and photosynthesis diminished, GPP gradually decreased to a low level. Across the growth period, GPP ranged from 0 to 14.07 g $C/m^2/d$, averaging a daily accumulation of 6.44 g $C/m^2/d$ and a cumulative total of 850.51 g C/m^2.

The NEP followed a trend similar to that of GPP but was also influenced by heterotrophic respiration. In the early growth stage, incomplete development of rice roots and leaves resulted in weak photosynthetic capacity and low heterotrophic respiration, leading to low NEP. During the rapid growth stage, increased leaf numbers and root development enhanced photosynthetic capacity, boosting NEP. Although heterotrophic respiration rose, it remained minor compared to photosynthate accumulation. In the reproductive growth stage, photosynthates were primarily allocated

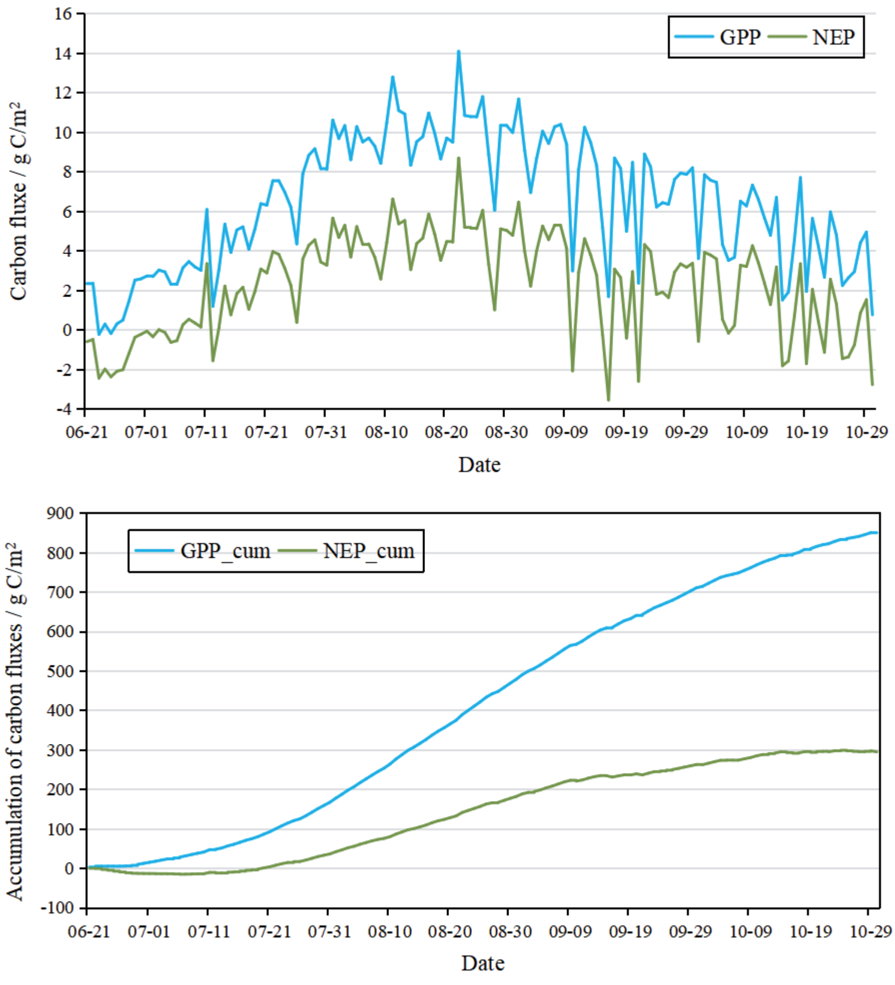

Fig. 5. Dynamic and cumulative changes in GPP and NEP.

to grain formation. Heterotrophic respiration stayed steady but was still minor relative to photosynthate accumulation, keeping NEP high. At maturity, as grains matured and photosynthesis declined, NEP gradually decreased. Heterotrophic respiration remained constant but was relatively large compared to the declining photosynthates, causing a rapid NEP decrease. Over the entire growth period, NEP ranged from -3.56 to 8.68 g C/m²/d, averaging 2.23 g C/m²/d, with a cumulative total of 294.36 g C/m².

Dynamic Changes in CH_4 Emission

Fig. 6 illustrates the dynamic and cumulative changes in CH_4 flux during the rice-growing season. Initially, during the seedling recovery stage, CH_4 emissions were low due to immature root systems and poor soil aeration. As rice progressed to the tillering stage, root development and field flooding created an anaerobic environment that stimulated methanogen activity, resulting in a gradual increase in CH_4 emissions, which peaked in early tillering. During the heading stage, when rice growth and root activity were at their peak, CH_4 emissions remained high. However, as rice matured, reduced root activity and field drainage-induced reoxygenation suppressed CH_4 emissions, leading to a gradual decline. Daily CH_4 emissions ranged from 0.02 to 1.19 g/m²/d, averaging 0.20 g/m²/d, with cumulative emissions reaching 27.05 g/m² over the growth period. A comparison of daytime and nighttime CH_4 emissions revealed similar patterns. Daily daytime emissions averaged 0.12 g/m²/d, totaling 15.64 g/m², while nighttime emissions averaged 0.09 g/m²/d, with a cumulative total of 11.41 g/m².

Variation in N_2O Emission

Fig. 7 depicts the variations in N_2O concentration, emission flux, and cumulative emissions across the rice-growing season. The average N_2O concentration over the entire period was 0.5472 ppm, with peaks following each nitrogen (N) fertilizer application. Specifically, the average concentrations were 0.5409 ppm (regreening), 0.5285 ppm (tillering), 0.6375 ppm (jointing-booting), 0.5975 ppm (heading-flowering), and 0.4803 ppm (milky stage), indicating higher levels during the reproductive growth stages.

The average N_2O emission flux was 2.5281 μg·m⁻²·h⁻¹, also peaking after N fertilization. Average fluxes were 0.3111 μg·m⁻²·h⁻¹ (regreening), 1.3412 μg·m⁻²·h⁻¹ (tillering),

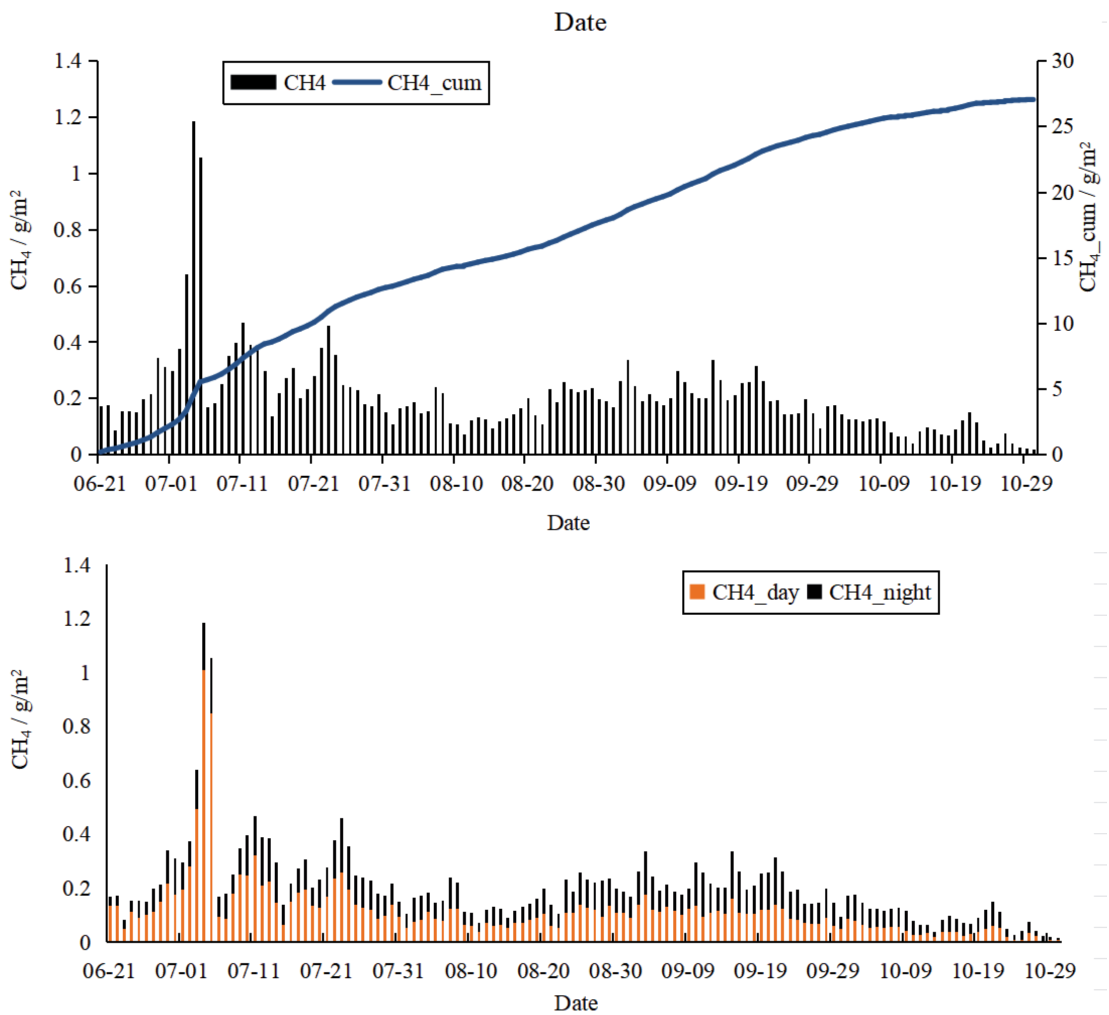

Fig. 6. Dynamic changes in CH_4 flux and comparison of daytime and nighttime CH_4 emissions.

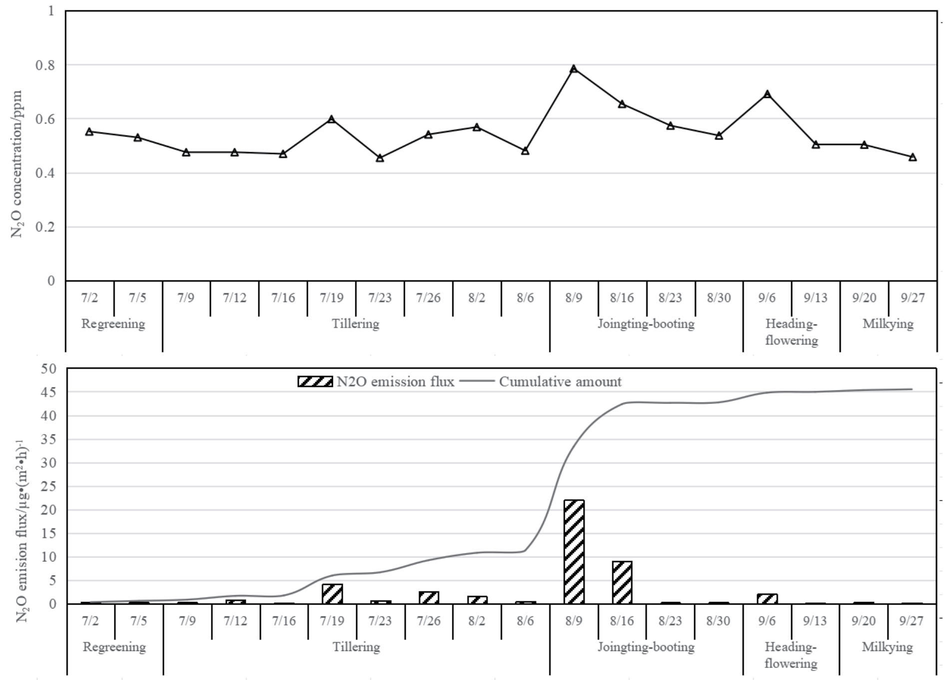

Fig. 7. Changes in N_2O concentration, emission flux, and cumulative amount.

7.8453 μg·m^{-2}·h^{-1} (jointing-booting), 1.1129 μg·m^{-2}·h^{-1} (heading-flowering), and 0.2743 μg·m^{-2}·h^{-1} (milky stage). Notably, N_2O emission fluxes surged from tillering to jointing-booting, with cumulative emissions also peaking during the jointing-booting stage.

Effects of Environmental Factors on Greenhouse Gas Emissions

Fig. 8 illustrates how GPP and NEP in rice fields respond to environmental factors over the growth period. Both GPP and NEP exhibited linear positive relationships with air temperature (Ta), soil temperature (Ts), and canopy temperature (T_leaf), increasing rapidly as these temperatures rose. From June to August, as temperatures climbed and rice grew vigorously, GPP and NEP reached their peaks. Subsequently, as temperatures declined, GPP and NEP gradually decreased until harvest, showing a similar pattern to temperature variations. However, while solar radiation also showed a relatively strong correlation with GPP and NEP, temperature alone had limited explanatory power. For instance, in summer, even with high temperatures but low solar radiation, GPP and NEP remained low. Overall, Ta, Ts, and T_leaf accounted for 17.43-42.20% of GPP variation and 15.61–32.16% of NEP variation.

As depicted in Fig. 8(g-i), both GPP and NEP exhibited a linear positive relationship with Photosynthetically Active Radiation (PAR), with daily values rising sharply as PAR increased. This was attributed to enhanced photosynthesis in rice leaves and greater daily carbon fixation under higher light intensity. Similarly, net crop carbon fixation also rose with increasing PAR. For Vapor Pressure Deficit (VPD), GPP and NEP initially increased and then declined, following a quadratic function pattern. GPP peaked at a VPD of 12.635 hPa, while NEP reached its maximum at 12.986 hPa, before both decreased. The figure also indicates that wind speed had a negligible impact on GPP and NEP, with NEP showing virtually no variation with wind speed changes.

Fig. 9 shows daily CH_4 emission responses to temperature and VPD across the growing season. CH_4 emissions rose linearly with temperature and VPD, increasing as air/soil temperature and VPD rose. However, temperature changes had minimal impact on CH_4, accounting for 15.12-17.37% of its variation. Similarly, VPD changes had little effect (R^2 = 0.1014), explaining 10.14% of CH_4 variation. In short, CH_4 emissions were somewhat related to temperature and VPD at different reproductive stages, but the effects were insignificant.

Structural equation modeling (SEM) is a method for establishing, estimating, and testing causal relationship models (Selonen, 2021). To explore how environmental factors affect greenhouse gas emissions under water-saving rice irrigation, SEM was used to analyze causal links among Ta, Ts, PAR, wind speed (v), GPP, NEP, CH_4, and N_2O emissions. Fig. 10 and Table 4 show the SEM and path analysis results, with all model-fit parameters meeting standards, indicating good model fit. The results indicated that VPD significantly reduced N_2O emissions and cumulative amounts, while PAR significantly increased both. Ta positively affected VPD and Ts, while v negatively affected N_2O but positively affected GPP. GPP positively influenced NEP, and N_2O positively affected GPP but negatively affected CH_4 emissions. Ts positively affected CH_4.

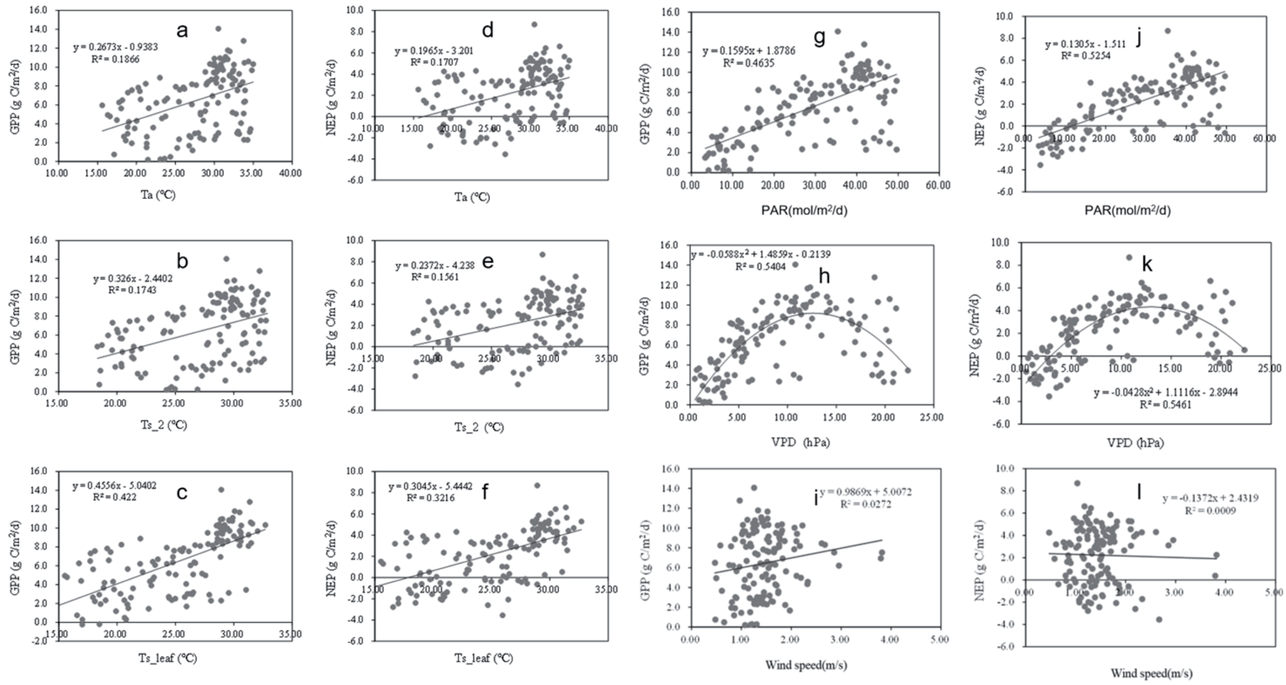

Fig. 8. Responses of GPP and NEP to environmental factors.

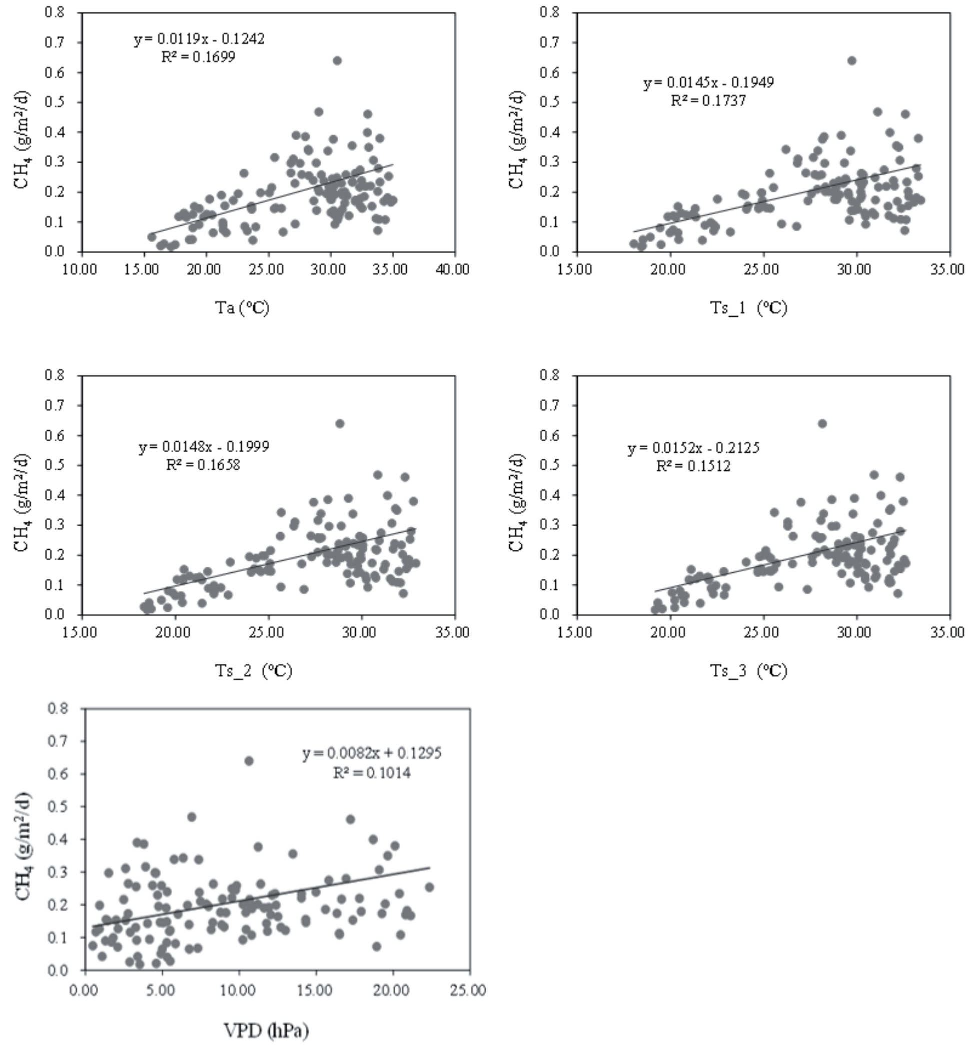

Fig. 9. Response of CH_4 emissions to environmental factors.

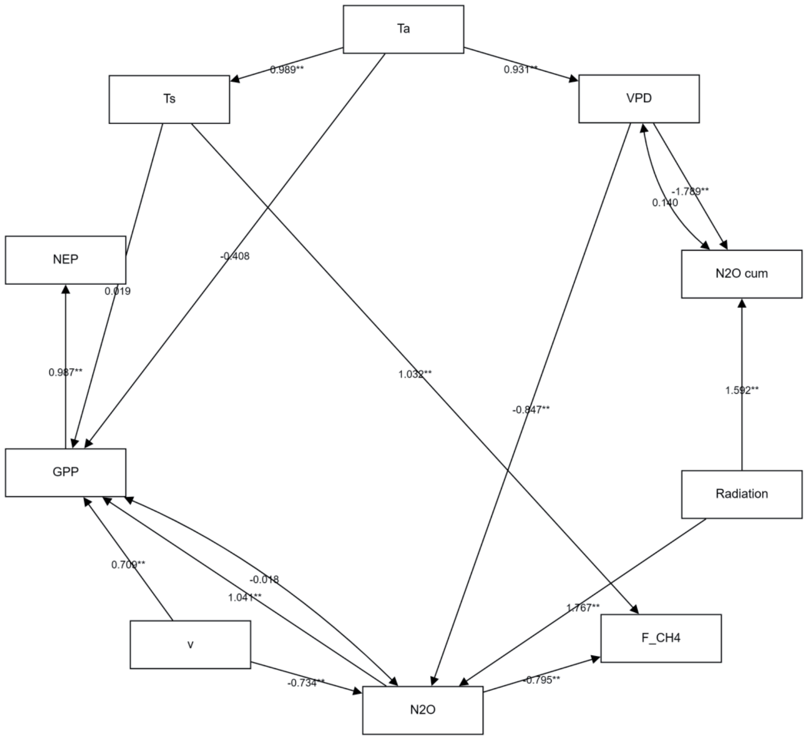

Fig. 10. Path relationships between environmental factors and greenhouse gas emissions (*P<0.05, **P<0.01).

Table 4. Fit indices of the structural model.

Indicator	χ2	df	p	χ²/df	GFI	RMSEA	TLI	CFI	AGFI	NNFI	PGFI
Standard values	-	-	>0.05	<3	>0.9	<0.10	>0.9	>0.9	>0.9	>0.9	>0.5
	32.57	32	0.439	1.018	0.999	0.06	0.992	0.995	0.999	0.992	0.581

Discussion

Interactions between Environmental Factors and N_2O Emissions

Under intermittent irrigation, environmental factors and greenhouse gas emissions interact in complex ways. Prior research has shown that CO_2 emission fluxes are significantly positively correlated with air temperature, and N_2O emission fluxes also display a marked positive linear correlation with air temperature [21]. A decline in vapor pressure deficit (VPD) boosts N_2O emissions and accumulation, likely due to VPD's impact on soil moisture and microbial activity. Soil moisture changes can modify microbial processes, making N_2O emissions sensitive to climatic conditions. VPD, in particular, governs N_2O production by influencing soil moisture and temperature, thus affecting nitrification and denitrification. In low-VPD (moist) conditions, continuous water films in soil pores enhance the activity of ammonia-oxidizing bacteria, raising N_2O flux. Increased radiation intensity also elevates N_2O emissions and accumulation. This could be because higher radiation raises soil temperature, speeding up nitrification and denitrification. Alternatively, it might increase rice transpiration, causing localized rhizosphere soil drying that promotes aerobic nitrification (a key N_2O source) while suppressing denitrification [22].

Prior research has revealed a notable positive correlation between N_2O emission flux and accumulated temperature. Solar radiation contributes to N_2O generation by photodecomposing soil-surface nitrate and dissolved organic nitrogen, yielding gases like NO and N_2O. Moreover, it can impair nitrite reductase enzymes (NirK/NirS) in denitrifying bacteria, causing N_2O to accumulate as an intermediate product during denitrification. Thus, solar radiation significantly impacts N_2O emissions [23]. Air temperature exerts positive effects on both VPD and soil temperature, indicating that rising air temperatures may elevate both simultaneously. Conversely, wind speed has a negative effect on N_2O emissions but a positive one on GPP, suggesting that moderate winds promote plant photosynthesis while inhibiting soil N_2O emissions. Nevertheless, some studies have found that higher wind speeds disrupt the soil-surface laminar boundary layer, markedly accelerating N_2O diffusion from soil pores into the atmosphere, with N_2O flux potentially increasing by 10-20% for every 1 m/s rise in wind speed [24].

Interactions between Environmental Factors and CH_4 And CO_2 Emissions

Low VPD signals ample atmospheric moisture, slowing water evaporation from plant leaves and supporting normal plant physiology and photosynthesis. As VPD moderately rises (air dries without harming plants), plants may optimize water use by adjusting stomatal aperture, enhancing photosynthetic efficiency and boosting GPP to some degree. Within an optimal VPD range, increased solar radiation and temperature elevate plant photosynthetic activity, enabling more light energy to be converted into chemical energy and raising GPP. However, once VPD surpasses a certain threshold, leaf water evaporation accelerates sharply, causing water imbalance and heightened water stress in plants. This disrupts photosynthesis and normal physiological functions, reducing GPP. To mitigate this, plants may close stomata to curb water loss, but this also limits CO_2 uptake, further hampering photosynthesis and GPP production.

In this study, GPP positively influenced NEP, suggesting that enhanced plant photosynthetic efficiency boosts NEP. This is consistent with prior research showing that a 1 g C/m^2 rise in GPP typically increases NEP by 0.6-0.8 g C/m^2, especially during the growing season [25]. Additionally, the positive impact of N_2O on GPP and its negative effect on methane (CH_4) highlight complex greenhouse gas interactions. Low-to-moderate N_2O emissions, often linked to increased ammonium nitrogen (NH_4^+) and nitrate nitrogen (NO_3^-) availability, can enhance plant photosynthesis and GPP. However, excessive N_2O emissions (e.g., post-fertilization peaks) may signal nitrogen saturation, causing leaching and suppressing GPP. The production of both N_2O and CH_4 depends on anaerobic conditions, and intensified denitrification (raising N_2O levels) may reduce CH_4 emissions. In intermittently irrigated rice fields, increased wet-dry cycling lowered CO_2 emissions during wet phases but raised total gas emissions compared to continuously moist controls [26]. The first wet-dry cycle triggered the highest cumulative soil CO_2 emissions, with soil moisture showing a strong positive correlation with CO_2 emission rates [27].

Differences in Agricultural Greenhouse Gas Emissions between Coastal and Inland Areas of Northern Zhejiang

Agricultural greenhouse gas emissions differ markedly between the coastal and inland regions of northern Zhejiang, shaped by farming practices, management, and climate [28]. Coastal emissions mainly stem from rice fields, with CH_4 contributing significantly, while inland areas see higher N_2O emissions, largely from nitrogen fertilizer use in upland crops like vegetables and fruits. Coastal soils are saline-alkali with high pH and unique organic carbon content, influencing microbial activity and carbon-nitrogen cycling. Lower average temperatures and higher wind speeds here may slow CH_4 production but enhance gas diffusion. Inland regions, dominated by well-drained red and rice soils with frequent wet-dry cycles, experience more active nitrogen transformations due to higher temperatures and sunlight, boosting N_2O emissions [29].

Given these differences, coastal mitigation strategies should prioritize optimizing water management, such as promoting water-saving irrigation practices and mid-season drainage to shorten continuous flooding periods. Improving saline-alkali soils through the application of organic matter or soil amendments and by adjusting pH can also curb CH_4 production. The intermittent irrigation used in this study effectively reduced CH_4 emissions [30]. Additionally, while this study found soil temperature positively influenced CH_4 emissions in rice fields, suggesting higher temperatures may promote CH_4 release, other research indicates that when soil moisture is stable, diurnal temperature variations have no significant impact on CH_4 flux [31], a finding supported by further studies [32].

This paper presents the results of only one year of experimental research. In the future, long-term continuous observations should be conducted to reveal the interannual variability patterns of greenhouse gas emissions and their responses to climate change. Concurrently, the approach should be validated and promoted at the regional scale, and carbon emission accounting methods should also be developed.

Conclusions

This study reveals the characteristics and interactions of greenhouse gas fluxes during rice growth. The main findings are as follows.

(1) GPP and NEP are significantly positively correlated and are mainly controlled by PAR (linear positive correlation) and VPD (quadratic correlation).

(2) The cumulative CH_4 emission was 27.05 g/m^2, peaking at the tillering stage under anaerobic conditions. CH_4 flux was positively correlated with soil temperature.

(3) The average N_2O flux was 2.5281 $\mu g \cdot m^{-2} \cdot h^{-1}$, peaking after nitrogen fertilization and during the jointing-booting stage. VPD had a significant negative effect on N_2O flux and cumulative emissions, while radiation showed a significant positive effect.

(4) N_2O significantly promotes GPP but inhibits CH_4 emissions, indicating trade-offs between carbon and nitrogen cycles.

Acknowledgments

This research was financially supported by Major Science and Technology Project of the Ministry of Water Resources (SKS-2025075),Provincial Research Institute Special Projects of Zhejiang Institute of Hydraulics and Estuary (Zhejiang Institute of Marine Planning and Design) (ZIHEYS25001), Water Conservancy Science and Technology in Zhejiang Province (RB2521, RC2527), and Basic Public Welfare Research Project of Zhejiang Province (LGN20E090001, LTGN24E090001). Deepseek was used only for grammatical polishing, sentence refinement, and academic expression optimization of the manuscript text. No AI-generated figures, tables, data predictions, or structured research conclusions were involved in this work.

AI Usage Disclosure Statement

No artificial intelligence tools were used for data generation, experimental design, result analysis, or core content creation of this study.

During the manuscript preparation process, general AI language tool (Deepseek) was used only for grammatical polishing, sentence refinement, and academic expression optimization of the manuscript text. No AI-generated figures, tables, data predictions, or structured research conclusions were involved in this work.

All content, research ideas, experimental schemes, data analysis processes, interpretation of results, and manuscript writing frameworks were independently completed, reviewed, verified, and revised by the authors. All AI-processed text has been fully checked, modified, and confirmed by the authors to ensure the accuracy, rationality, and scientific rigor of all statements, data, and conclusions in the final manuscript.

All raw data underlying the findings of this study are complete, authentic, and reproducible. The authors guarantee that all results presented in this manuscript can be fully verified and repeated.

The authors confirm that this declaration accurately describes the scope, content, and timeline of AI involvement in this research and manuscript preparation.

Conflict of Interest

The authors declare no conflict of interest

References

1. ZHANG W. Regulation and mechanism of greenhouse gas emission from rice field farming combined with recycling agriculture. Shanxi Chemical Industry, **40** (60, **2020** [In Chinese].
2. WANG J., LIU W., HAO X., ZHANG S., HE D., ZHANG X., ZHOU L. Effects of biochar and nitrogen fertilizer on CO_2 and N_2O emissions from cotton fields at different temperatures. Journal of Agriculture, **14** (12), 19, **2024** [In Chinese].
3. LIU Q., HEN X., NIU J., XU Y., JIANG J. Research progress on soil habitat changes and CO_2 and CH_4 production and emission characteristics under flooding stress. Water Saving Irrigation, **12**, 89, **2025** [In Chinese].
4. RUNKLE R., SUVOCAREV K., REBAM M., REAVIS C., SMITH S., CHIU Y., FONG B. Methane emission reductions from the alternate wetting and drying of rice fields detected using the eddy covariance method. Environmental Science & Technology, **53**, 671, **2019**.
5. FENG S., HE J., WANG Y., CHEN Z., YE L., ZHANG H., ZHANG J., RONG L., LUO W. Study on rain-storage intermittent irrigation regimes for rice based on entropy weight TOPSIS method. Water Saving Irrigation, **11**, 80, **2025** [In Chinese].
6. YAN Y., XU T., XIE H., XU K., CHEN J., LIU B. Effects of organic fungal fertilizer coupled with alternate wetting and drying irrigation on weed community diversity in a double-season rice field. Water Saving Irrigation, **10** (31), 49, **2025** [In Chinese].
7. CHEN M, LI Z.W., NIE X.Z., WANG S.L., RAN F.W., CHEN Y. Current status and prospects of terrestrial ecosystem carbon sink in the Dongting Lake Basin, China. Chinese Journal of Applied Ecology, **36** (11), 3501, **2025** [In Chinese].
8. MING G.H., HU H.C., TIAN FU.Q. Carbon budget for a plastic-film mulched and drip-irrigated cotton field in an oasis of Northwest China. Agricultural and Forest Meteorology, **306**, 108447, **2021**.
9. WAGLE P., GOWDA P.H., NORTHUP B.K. Carbon dioxide and water vapor fluxes of multi-purpose winter wheat production systems in the U.S. Southern Great Plains. Agricultural and Forest Meteorology, **310**, 108631, **2021**.
10. MONTAGNANI L., ZANOTELLI D., TAGLIAVINI M., TOMELLERI E. Timescale effects on the environmental control of carbon and water fluxes of an apple orchard. Ecology and Evolution, **8** (1), 416, **2017**.
11. SONG C.Q., LIU W., LU H.B., YUAN W.P. Characteristics and drivers of methane fluxes from a rice paddy based on the flux measurement. Advances in Earth Science, **34** (11), 1141, **2019** [In Chinese].
12. SHI Y.Z., CUI Y.L., CAI S., HONG D.L., CHENG J. CH_4 fluxes and their comprehensive greenhouse effects with CO_2 fluxes in direct-seeded rice in Poyang Lake Plain. Environmental Science, **44** (3), 1572, **2023** [In Chinese].
13. ZHOU D., LIU M., ZHANG Z., ZOU S., NI M., YUAN J. Research on greenhouse gas emissions reduction and influencing factors of Micropterus salmoides Inner-Pond Raceway Aquaculture. Journal of Aquatic Ecology, **47** (04), 67, **2024**.
14. ZHANG Z., LIU M., ZHOU D., GUO A., LIAN Q, LUO K., XU Q., CHEN G., YUAN J. Spatio-temporal emission characteristics and environmental factors of greenhouse gases in Qianxiahu Reservoir. Acta Scientiae Circumstantiae, **44** (7), 388, **2024** [In Chinese].
15. GUNTIÑAS M., LEIROS M., TRASAR-CEPEDA C., GIL-STOTRES F. Effects of moisture and temperature on net soil nitrogen mineralization: a laboratory study. European Journal of Soil Biology, **48**, 73, **2011**.
16. YAN Y., LI S., WANG S., CAO Z., CAO Q., ZUO Q., CHEN M. Response of spatiotemporal variation in soil N_2O emissions from nitrification to the restoration of degraded tropical forests. Ecology and Environmental Sciences, **34** (12), 1879, **2025** [In Chinese].
17. LI Y., ZHENG S., XIAO M., XIA Y., WANG W., CAI J. Effect on physiological growth and water utilization of rice under different varieties and irrigation modes. Polish Journal of Environmental Studies, **31** (6), 5125, **2022**.
18. XIAO M., LI Y., LU B. Response of net photosynthetic rate to environmental factors under water level regulation

in paddy field. Polish Journal of Environmental Studies, **28** (3), 1, **2019**.
19. XIAO M., LI Y., JIA Y., WANG J. Effect on water consumption and non-point source pollutants loss under different water and nitrogen regulation of paddy field in Southern China. Polish Journal of Environmental Studies, **31** (2), 1389, **2022**.
20. XIAO M., LI Y., JIA Y., WANG J. Mechanism of water savings and pollution reduction in paddy fields of three typical areas in southern China. International Journal of Agricultural and Biological Engineering. **15** (1), 199, **2022**.
21. ZHOU W.C., XIANG S.S., OU W.H., XU X.H., SHI Y.H., ZUO Y.X. Greenhouse gas emissions and their controlling factors in a Hong Lake shore zone in middle reaches of the Yangtze River. Acta Scientiae Circumstantiae, **45**, 458, **2025** [In Chinese].
22. HU B., WANG Y., ZHAO H., WANG C., SHI Z. Effects of surface wind speed and simulated precipitation on N_2O emissions during dairy manure stacking. Transactions of the Chinese Society of Agricultural Engineering, **36** (07), 232, **2020** [In Chinese].
23. MA L., LOU Y., WANG Y., YANG X., LI J., MA Y., SHA H., LI R., ZHANG Z. Effects of sowing dates on N_2O emissions from winter wheat fields under different shading conditions. Remote Sensing Technology and Application, **38**, 1390, **2023** [In Chinese].
24. GAO X.A., ZHU L.Y., YAN S.M., PEI K.N., ZHANG F.S., WANG S.M., CHENG P.W. Spatio-temporal distribution characteristics and influencing factors of greenhouse gases in Linfen, a typical high-carbon-emission City. Journal of Arid Meteorology, **40**, 256, **2022** [In Chinese].
25. LUO X., KEENAN T.F. Tropical extreme droughts drive long-term increase in atmospheric CO_2 growth rate variability. Nature Communications, **13**, 1193, **2022**.
26. OUYANG Y., LI X. Impacts of drying - wetting cycles on CO_2 and N_2O emissions from soils in different ecosystems. Acta Ecologica Sinica, **33**, 1251, **2013** [In Chinese].
27. BAO Z., HOU Y., ZHU X., ZHAO C., HU B., JIA H., XU X. Effect of alternating wetting and drying and simulated nitrogen deposition on soil CO_2 emission in alpine wetlands of Bayinbulak. Journal of Agro-Environment Science, **37** (03), 598, **2018** [In Chinese].
28. LI Y., ZUO L.J. Assessment of greenhouse gas emissions and changes in China's crop farming sector, 2000 to 2020. Journal of Agricultural Resources and Environment, **42** (6), 1493, **2025** [In Chinese].
29. FAN Z., QI X., ZENG L., WU F. Accounting of greenhouse gas emissions in the Chinese agricultural system from 1980 to 2000. Acta Ecologica Sinica, **42**, 9470, **2022** [in Chinese].
30. PRASTIYO S.E., IRHAM, HARDYASTUTI S., JAMHARI. How agriculture, manufacture, and urbanization induced carbon emission? The case of Indonesia. Environmental Science and Pollution Research, **27**, 42092, **2020**.
31. WEI D., XU R., WANG Y., YAO T. CH_4, N_2O and CO_2 fluxes and correlation with environmental factors of alpine steppe grassland in Nam Co region of Tibetan plateau. Acta Agrestia Sinica, **19**, 412, **2011** [In Chinese].
32. HAO Q., WANG Y., SONG C., WANG Y., WANG M. Primary study on CO_2 and CH_4 emissions from wetland soils in the Sanjiang plain. Journal of Agro-Environment Science, (05), 846, **2004**.